Defects Passivation With Dithienobenzodithiophene-based π-conjugated Polymer for Enhanced Performance of Perovskite Solar Cells

Xianqiang Li, Wenhui Li, Yijie Yang, Xue Lai, Qiang Su, Dan Wu, Gongqiang Li, Kai Wang, Shuming Chen, Xiao Wei Sun, and Aung Ko Ko Kyaw**

A dithienobenzodithiophene-based π-conjugated polymer consisting of fluorinated benzotriazole and benzothiadiazole is successfully applied through anti-solvent method to passivate the defects of perovskite crystals. The fluorinated polymer interacts with under coordinated Pb^{2+} ions in the perovskite crystals to form Pb-F bond which effectively passivates the defects. The trap density is reduced and the charge carrier transfer between the perovskite film and Spiro-OMeTAD is also improved after passivation with the polymer. As a result, a power conversion efficiency (PCE) of 18.03% is achieved in the champion cell. After storing in an ambient environment with 60% relative humidity for 1000 h, the device still retains 90% of the original PCE. These results demonstrate that dithienobenzodithiophene-based π-conjugated polymers are promising materials for passivation of perovskite films to further improve the performance and stability of perovskite solar cells.

1. Introduction

In recent years, a new emerging photovoltaic technology, which uses the solution-processed organic–inorganic lead halide perovskite as a light absorber, has attracted lots of attentions. Compared to the dominant photovoltaic technology based on inorganic materials such as Si and GaAs, the perovskite solar cells (PSCs) have several advantages: low-cost fabrication process, mechanical flexibility, solution processability, and compatibility with roll-to-roll fabrication process.[1–3] Moreover, the power conversion efficiency (PCE) of PSCs experienced a skyrocketing increase. In just within a decade, the PCE was enhanced from 3.8% in 2009[4] to 23.7% recently.[5] Despite the rapid development, the commercialization of PSC is still challenging. In most of the PSCs, the perovskite films are prepared by solution processes, such as one-step spin coating,[6,7] sequential deposition,[8] vapor assisted solution process,[9] etc. However, the solution-processed polycrystalline perovskite films contain lots of defects at the surface and grain boundaries (GBs) although bulk-defect is not serious owing to its defect tolerance nature arrives from the low crystallization temperature. In the polycrystalline perovskite films, the defects could form electronic trap states,[10–12] limit lateral diffusion of carriers,[13] reduce charge carrier lifetime, and cause ion diffusion and migration,[14,15] thus limiting the efficiency and stability of PSCs. Therefore, passivating defects at the surface and GBs within perovskite films becomes important for achieving the high performance of PSCs.[16–18]

Among the various perovskite deposition techniques, one-step spin coating technique with anti-solvents (chlorobenzene (CB), toluene, etc.) has been widely used for achieving the high-efficiency PSCs because it is one of the effective methods and can produce uniform and high-quality perovskite films.[19–22] However, efforts must be made to suppress the defects to further improve the performance and stability of PSCs. D. Bi et al. introduced an insulator, PMMA, into anti-solvent (CB/toluene) to enable much faster heterogeneous nucleation of perovskite crystals, thus resulting in smooth perovskite films with fewer defects and larger oriented grains.[23] Wu et al. used [6,6]-phenyl-C61-butyric acid methyl ester (PCBM) in toluene as

Dr. X. Li[+], Dr. W. Li[+], Dr. Y. Yang, X. Lai, Q. Su, Dr. D. Wu, Prof. K. Wang, Prof. S. Chen, Prof. X. W. Sun, Prof. A. K. K. Kyaw
Guangdong University Key Laboratory for Advanced Quantum Dot Displays and Lighting
Department of Electrical & Electronic Engineering
Southern University of Science and Technology
Shenzhen 518055, P. R. China
E-mail: aung@sustc.edu.cn

X. Lai, Prof. G. Li
Key Laboratory of Flexible Electronic (KLOFE) & Institute of Advanced Materials (IAM)
Jiangsu National Synergistic Innovation Center for Advanced Materials (SICAM)
Nanjing Tech University
30 South Puzhu Road, Nanjing 211816, P. R. China
E-mail: iamgqli@njtech.edu.cn

Prof. K. Wang, Prof. X. W. Sun, Prof. A. K. K. Kyaw
Shenzhen Planck Innovation Technologies Pte Ltd.
Ganli 6th Road, Longgang, Shenzhen 518112, P. R. China

The ORCID identification number(s) for the author(s) of this article can be found under https://doi.org/10.1002/solr.201900029.

[+]Dr. X. Li and Dr. W. Li contributed equally to this work.

DOI: 10.1002/solr.201900029

anti-solvent to form the graded heterojunction structure which could improve the photoelectron collection and reduce recombination loss.[7] In addition to insulating polymer and fullerene, semiconducting polymers also could protect and passivate the perovskite crystals, regardless of p-type or n-type property.[24] Recently, a champion polymer used in organic solar cells, poly[(2,6-(4,8-bis(5-(2-ethylhexyl)thiophe-2-yl)-benzo[1,2-b:4,5-b']dithiophene))-alt-(5,5-(1',3'-di-2-thienyl-5',7'-bis(2-ethylhexyl) benzo[1',2'-c:4',5'-c']dithiophene-4,8-dione))] (PBDB-T), exhibited a good passivation effect in perovskite crystals when the polymer dissolved in CB was used as an anti-solvent.[25,26] The hydrophobic p-type π-conjugated PBDB-T not only facilitates the formation of high-quality, smooth and uniform perovskite films, but also passivates the surface defects of perovskite through the formation of Lewis adduct between perovskite and PBDB-T. Although these investigations demonstrated that incorporating polymeric semiconductors into anti-solvents is a promising method for improving PSCs performance, more in-depth studies are required to understand the underlying mechanisms for the performance improvement.

Different than prior reports, herein we used a wide bandgap dithienobenzodithiophene-based π-conjugated polymer PDTBDT-FBT[27,28] (See **Figure 1** for the chemical structure) dissolved in CB as an anti-solvent (hereafter we called it "polymer containing anti-solvent") and investigated its influence on the perovskite crystals and device performance. There are several reasons that we chose the PDTBDT-FBT in CB as anti-solvent. Firstly, the HOMO level of PDTBDT-FBT is very deep (−5.51 eV), while that of Spiro-OMeTAD is −5.22 eV. Thus, incorporating PDTBDT-FBT in CB as anti-solvent can not only passivate the defects, but also facilitate holes to transport from perovskite to Spiro-OMeTAD. Second, the electron-accepting moiety, 5,6-difluorobenzo[c][1,2,5]thiadiazole (FBT), in PDTBDT-FBT might coordinate Pb ions or defects in the perovskite film, thus improving charge carrier transport properties. In addition, PDTBDT-FBT has a high hole mobility of 0.1 $cm^2 V^{-1} S^{-1}$,[27] which could also help to improve the performance of PSC. By using the polymer containing anti-solvent, a PCE of 18.03% was achieved in the champion device. The average PCE (obtained from at least 20 devices) of PSCs prepared by the polymer containing anti-solvent is as high as 16.19% whereas that of PSCs prepared by the pure CB anti-solvent is only 14.91%. The characterization results revealed that fluorinated PDTBDT-FBT participates in the perovskite crystal growth process, anchors at the surface and GBs of perovskite film and passivates the defects by the formation of Pb-F bound. The improved performance of PSCs with negligible hysteresis demonstrates that perovskite crystals can be effectively passivated by incorporating PDTBDT-FBT polymer into conventional CB anti-solvent. The passivation effect of PDTBDT-FBT on perovskite films could also improve the stability of PSC in ambient environment.

2. Results and Discussion

Figure 1a shows the device structure and cross-section Scanning Electron Microscopy (SEM) image of PSC. The PSC has a regular structure which consists of FTO bottom electrode, TiO_2 compact layer, TiO_2 mesoporous layer, perovskite film, Spiro-OMeTAD,

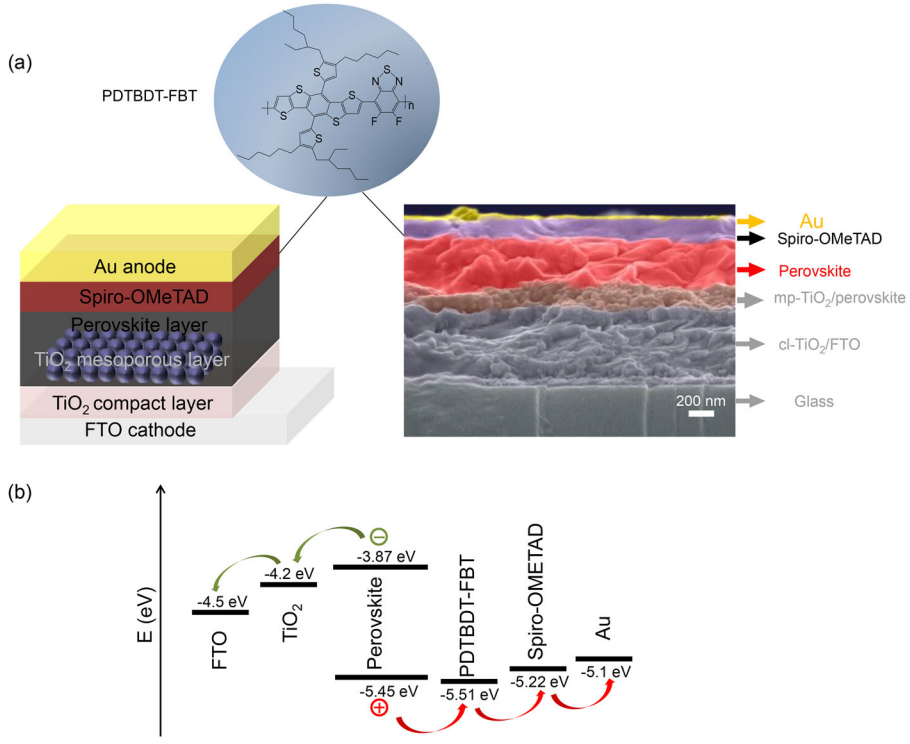

Figure 1. a) Device structure and cross-section SEM image of PSC with the chemical structure of PDTBDT-FBT. b) Energy level diagram of PSCs.

and Au top electrode. The perovskite film was prepared by spin coating a precursor solution containing CsI, PbI_2, FAI, $PbBr_2$, and MABr, and polymer containing anti-solvent with various concentrations of PDTBDT-FBT. The detailed fabrication process can be found in the Experimental Section. The energy level diagram of the PSC is shown in Figure 1b. The HOMO level of PDTBDT-FBT (−5.51 eV) matches well with the valence band maximum of the perovskite (−5.45 eV).

The *J-V* characteristics of PSCs prepared by polymer containing anti-solvent with different concentrations of PDTBDT-FBT are shown in **Figure 2**a and the detailed photovoltaic parameters are shown in **Table 1**. The *J-V* characteristics are extracted from the devices whose PCEs are similar to the average values. Compared to the PCE of controlled device prepared by the pure CB anti-solvent (16.85%, average 14.91%), introducing PDTBDT-FBT with concentration of 0.5 and 1 mg mL^{-1} improved the PCE to 17.56% (average 15.51%) and 18.03% (average 16.19%), respectively. However, further increase in the concentration of PDTBDT-FBT decreased the PCE to 11.44% (average 10.73%) and 8.01% (average 7.56%) for 2 and 5 mg mL^{-1}, respectively. Therefore, the best performance was obtained when the concentration of PDTBDT-FBT in CB is 1 mg mL^{-1} (The concentration of PDTBDT-FBT hereafter refers to 1 mg mL^{-1} unless otherwise stated). The external quantum efficiency (EQE) spectra of the PSCs with average performance are shown in Figure 2b. The EQE of PSC prepared by the polymer containing anti-solvent is higher than that of the PSC prepared by the CB anti-solvent in the wavelength range from 300 to 500 nm. The *J-V* characteristic and photovoltaic parameters of the champion PSC prepared by the polymer containing anti-solvent are shown in Figure 2c. The highest PCE of 18.03% was obtained with V_{oc} of 1.11 V, J_{sc} of 21.62 mA cm^{-2} and FF of 75.14%. To examine the reproducibility of our experiment, we fabricated at least 20 devices for each anti-solvent treatment. The statistics of PCE are shown in Figure 2d. The statistics of detailed photovoltaic parameters of PSCs (J_{sc}, V_{oc}, and *FF*) are shown in Figure S1, Supporting Information. The average PCE of PSCs prepared by the polymer containing anti-solvent is 16.19 % while that of PSCs prepared by the CB anti-solvent is only 14.91%. All *J-V* characteristics and photovoltaic parameters shown in Figure 2 were obtained under reverse voltage scan direction. The devices were also measured under forward voltage scan direction; the *J-V* characteristics and photovoltaic parameters are shown in Figure S2 and Table S1, Supporting Information. We observed that the hysteresis effect in the PSCs prepared by the polymer containing anti-solvent was negligible and much smaller than that in the PSCs prepared by the CB anti-solvent.

The statistical data clearly showed that introducing dithienobenzodithiophene-based π-conjugated polymer in the conventional anti-solvent improves the PCE of PSC. However, the concentration of PDTBDT-FBT in CB anti-solvent should be carefully optimized; otherwise the PCE will be reduced. To understand the underlying passivation mechanism, we first measured the absorption spectra of perovskite films prepared by two different methods: the polymer containing anti-solvent and the pure CB anti-solvent (**Figure 3**a). Both perovskite films have a similar absorption property in the range from 550 to 800 nm, but the perovskite film prepared by the polymer containing anti-solvent exhibits a higher absorption in the range from 400 to 550 nm. The UV-vis absorption measurement results agree with the EQE measurement (Figure 2b). The higher EQE of PSCs

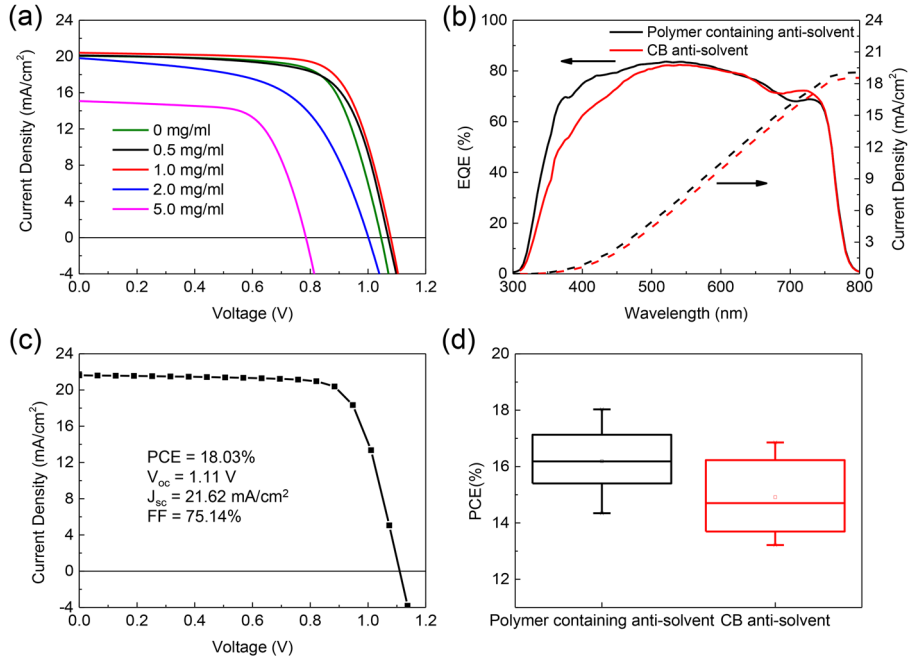

Figure 2. a) *J–V* characteristics of PSCs prepared by polymer containing anti-solvent with different concentrations of PDTBDT-FBT under AM 1.5 G illumination. b) EQE spectra of PSCs prepared by the CB anti-solvent and by the polymer containing anti-solvent. c) *J–V* characteristic of the champion device prepared by the polymer containing anti-solvent. d) PCE statistics of PSCs prepared by the polymer containing anti-solvent and by the CB anti-solvent. The concentration of PDTBDT-FBT used for polymer containing anti-solvent in b), c) and d) is 1 mg mL^{-1}.

Table 1. Photovoltaic parameters of PSCs.

Concentration of PDTBDT-FBT in CB	V_{oc} [V]	J_{sc} [mA cm^{-2}]	FF [%]	Average PCE [%]*	Best PCE [%]
0 mg mL^{-1}	1.060 ± 0.05	19.910 ± 0.47	69.724 ± 0.03	14.911 ± 0.22	16.85
0.5 mg mL^{-1}	1.070 ± 0.03	20.410 ± 0.51	70.883 ± 0.30	15.511 ± 0.05	17.56
1 mg mL^{-1}	1.090 ± 0.04	20.340 ± 0.38	71.923 ± 0.36	16.191 ± 0.06	18.03
2 mg mL^{-1}	1.000 ± 0.04	19.430 ± 0.80	54.033 ± 0.24	10.730 ± 0.71	11.44
5 mg mL^{-1}	0.790 ± 0.03	15.080 ± 0.83	63.604 ± 0.23	7.560 ± 0.57	8.01

* The average PCE was obtained from at least 20 cells

prepared by the polymer containing anti-solvent should be attributed to the stronger absorption of the perovskite film, which may be related to the morphology change in the perovskite film induced by the polymer containing anti-solvent.

Figure 3b shows the XRD spectra of the perovskite films prepared by two different methods on FTO substrates with compact TiO_2 and mesoporous TiO_2 layers. The characteristic peaks for a trigonal perovskite phase can be clearly observed at 14.12°, 20.00°, 24.58°, 28.44°, 31.88°, 35.00°, 40.64°, 43.20°, and marked with (−111), (−120), (021), (−222), (−231), (030), (−240), (−333). The peak at 12.70° arrives from the (001) lattice planes of PbI_2.[19,23] Compared to the perovskite film prepared by the CB anti-solvent, the perovskite film prepared by the polymer containing anti-solvent has more oriented crystals indicated by the larger peak intensity ratio of (−111) to (−231). Similar phenomenon has been reported before.[23] This is because the (−111)-oriented grains grow faster by consuming neighboring non-oriented crystals, which could be attributed to the polymer containing anti-solvent induced grain attachment.

We also carried out the XPS measurement to examine the interaction of PDTBDT-FBT with perovskite film. The XPS Pb 4f spectra are shown in Figure 3c. The binding energies of Pb 4f7/2 and Pb 4f5/2 are 138.5 and 143.4 eV, respectively, in the perovskite film prepared by the CB anti-solvent whereas that of Pb 4f7/2 and Pb 4f5/2 are 138.3 and 143.1 eV, respectively, in the perovskite film prepared by the polymer containing anti-solvent, exhibiting a shift in binding energy. Many research groups have reported that interaction between perovskite and other materials could lead to changing surface states of perovskite films and Pb 4f binding energy.[29–31] Zhang et al. observed the Pb 4f binding energy shifted to a lower value after introducing Poly[N-9'-heptadecanyl-2,7-carbazole-alt-5,5-(4',7'-di-2-thienyl-2',1',3'−benzothiadiazole)] (PCDTBT) into perovskite film.[29] Privitera et al. found that introducing Poly(3-hexylthiophene-2,5-diyl) (P3HT) into perovskite to form nanocomposite could lead to reducing the binding energy of Pb 4f, which is attributed to the excess of negative charges on the perovskite/P3HT nanocomposites due to an electronic interaction between the

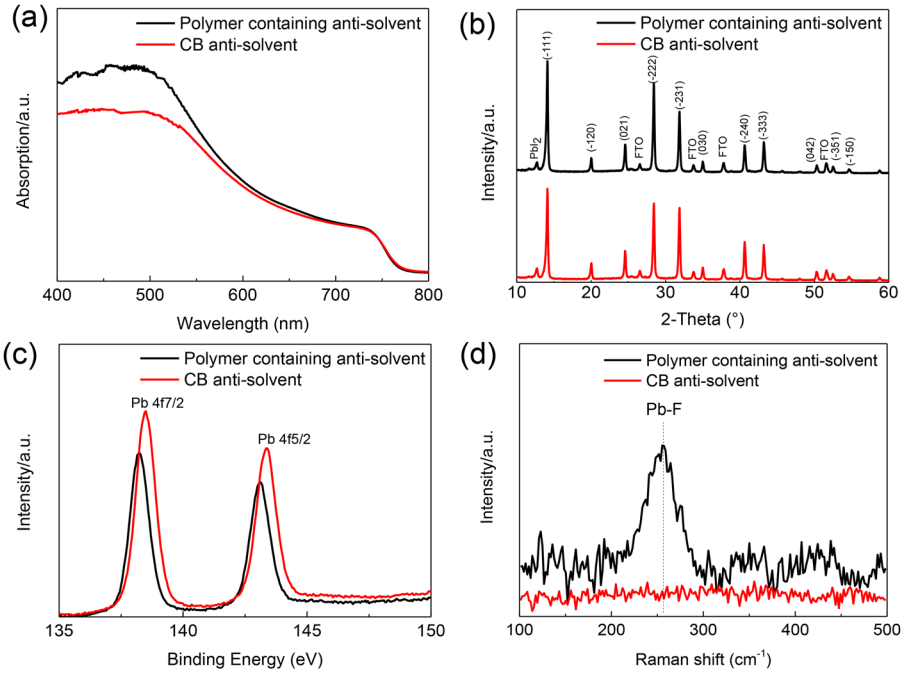

Figure 3. a) UV-vis absorption spectra, (b) XRD patterns, (c) XPS Pb 4f, and (d) Raman spectra for perovskite films prepared by the polymer containing anti-solvent (1 mg mL^{-1} PDTBDT-FBT in CB) and by the CB anti-solvent.

perovskite and the P3HT.[30] In our study, the shift in binding energy of Pb 4f to lower values is a good evidence of interaction between PDTBDT-FBT and under-coordinated Pb in the perovskite film. Moreover, Fourier-transform infrared spectroscopy (FTIR) measurement results also confirmed the existence of F in perovskite film (see Figure S3, Supporting Information). Raman spectra were applied to obtain the bonding information between PDTBDT-FBT and under-coordinated Pb^{2+} ions. As shown in Figure 3d, we observed a low frequency Raman band at $\approx$255 cm^{-1}, which can be assigned to the vibration of Pb-F bond.[32,33] The combined analysis of XPS, FTIR and Raman show the direct evidence that interaction between the F atoms in PDTBDT-FBT and under-coordinated Pb^{2+} ions in the perovskite forms the Pb-F bound which effectively passivate the defects associated with Pb^{2+} vacancies.

To figure out how PDTBDT-FBT influenced the perovskite crystals, we used SEM measurement to investigate the surface morphology of perovskite films as shown in **Figure 4**. In the perovskite film prepared by the CB anti-solvent (Figure 4a), the GBs of perovskite crystals can be clearly observed. In contrast, the GBs become less apparent and the perovskite crystals become more homogeneous in the perovskite film prepared by the polymer containing anti-solvent although the grain sizes in the two types of films look similar (Figure 4b). To confirm this, we also obtained the average grain sizes in perovskite films from the SEM image in Figure 4. The SEM images of the perovskite films marked with sizes of some grains and the crystal size statistics (obtained from at least 80 crystals using Nano Measure Software) are shown in Figure S4, Supporting Information. The average grain sizes in the perovskite film prepared by the CB anti-solvent and the polymer containing anti-solvent are 314.5 and 319.0 nm, respectively. The very similar grain sizes in both perovskite films indicate that the polymer containing anti-solvent does not affect the grain size of the perovskite film despite an apparent change in morphology.

We also used EDX measurement to study the distribution of PDTBDT-FBT on the surface of perovskite film. Figure 4c,d are EDX F and Pb mapping of perovskite film prepared by the polymer containing anti-solvent. The Pb elements which represent perovskite are homogeneously and densely distributed everywhere on the perovskite film whereas F elements which present PDTBDT-FBT are located only at localized surface and GBs, where the defects are likely to be present. The F and Pb element distributions reveal that the passivation of PDTBDT-FBT occurs mainly at the GBs and the localized surface.

The negligible hysteresis in *J–V* curve of the PSC prepared by the polymer containing anti-solvent also suggests less crystal defects in perovskite film due to the passivation. Dense and uniform perovskite film usually exhibits stronger absorbance in the visible wavelength range.[34–36] In addition, imperfections such as domain walls within crystals or surface defects, and crystallinity could influence the nature and dynamics of photophysical mechanisms.[37] Therefore, the SEM image of the perovskite film prepared by the polymer containing anti-solvent film, which exhibits less apparent grain boundaries and denser film, is in good agreement with the UV-vis absorption spectra in Figure 3a, in which the perovskite film prepared by the polymer containing anti-solvent has a stronger absorbance than the one prepared by the CB anti-solvent does in the visible wavelength range.

Time-resolved photoluminescence (TrPL) measurement was carried out to further investigate the influence of PDTBDT-FBT passivation on the charge transport properties in perovskite films as shown in **Figure 5**. The samples for TrPL measurement

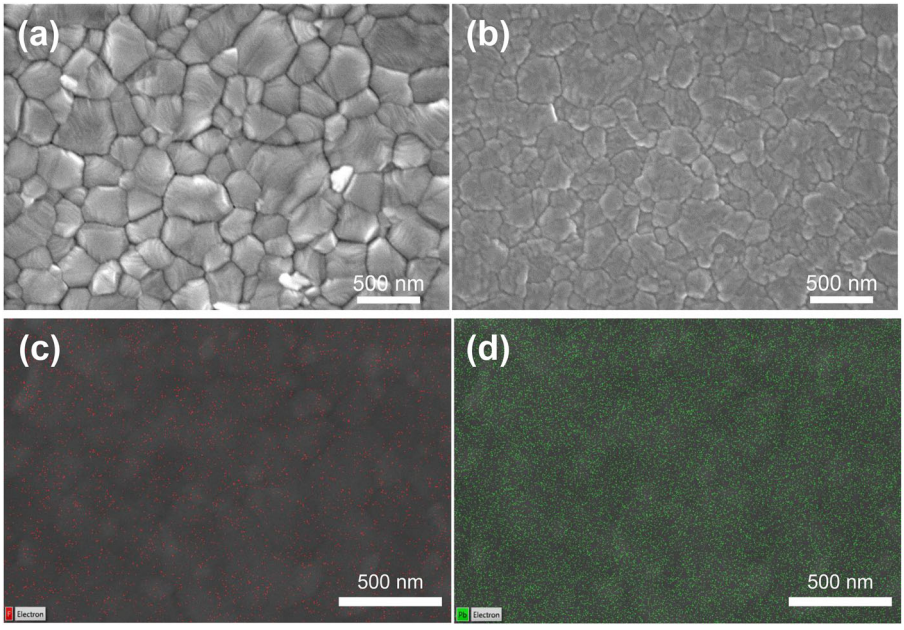

Figure 4. SEM images of surface of perovskite films prepared by (a) the CB anti-solvent and, (b) the polymer containing anti-solvent. c) Fluorine and (d) lead EDX mapping of perovskite film prepared by the polymer containing anti-solvent. The concentration of PDTBDT-FBT used for the polymer containing anti-solvent is 1 mg mL^{-1}.

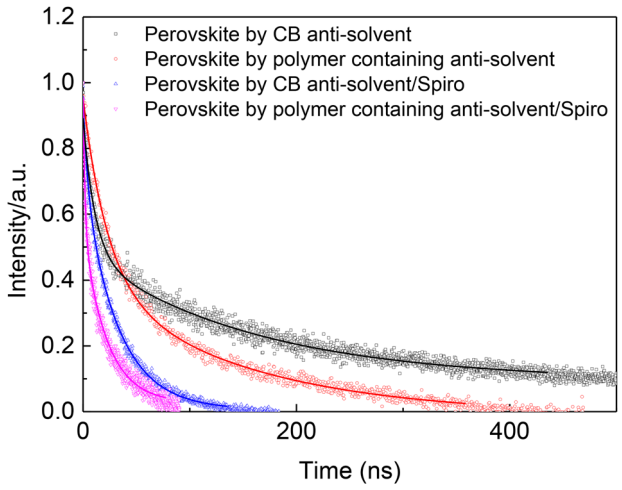

Figure 5. TrPL spectra of samples with a structure of glass/perovskite or glass/perovskite/Spiro-OMeTAD. The perovskite films were prepared by the polymer containing anti-solvent (1 mg mL^{-1} PDTBDT-FBT in CB) or the CB anti-solvent.

were prepared on the glass substrates with the structures of glass/perovskite or glass/perovskite/Spiro-OMeTAD. We fitted the PL decay curves by using a bi-exponential decay function as shown below:[38]

$$I(t) = A_1 \exp\left(-\frac{t}{\tau_1}\right) + A_2 \exp\left(-\frac{t}{\tau_2}\right)$$

where the smaller time constant τ_1 represents bimolecular recombination, the larger time constant τ_2 represents the charge carriers lifetime of perovskite film, and A_1 and A_2 represent PL decay amplitudes. **Table 2** shows the PL decay times and the decay amplitudes obtained by fitting the PL decay curves. The PL decay curve of the perovskite film prepared by the CB anti-solvent has a decay time of 161.37 ns. In contrast, the PL decay of perovskite film prepared by the polymer containing anti-solvent has a decay time of 147.08 ns. The shorter PL decay time in the perovskite film prepared by the polymer containing anti-solvent suggests that there is a charge transfer between the perovskite crystal and PDTBDT-FBT. The sample with a structure of glass/perovskite/Spiro-OMeTAD prepared by the polymer containing anti-solvent also has a faster decay time (21.99 ns) than the one prepared by the CB anti-solvent does (31.88 ns). The fast PL decay time indicates more efficient charge transfer at the interface between perovskite film and Spiro-OMeTAD. This could be attributed to the passivation effect of PDTBDT-FBT on crystal defects which could trap charge carriers and impede charge transfer. Besides, the charge carriers might transfer from perovskite film to PDTBDT-FBT first and then to Spiro-OMeTAD. Compared to the direct charge transfer from perovskite film to Spiro-OMeTAD, the two-step charge transfer process is more efficient as indicated by the shorter PL decay time.

To further investigate the passivation effects of the PDTBDT-FBT, we carried out the space-charge-limited-current (SCLC) analysis on the hole-only device with a structure of FTO/PEDOT:PSS/perovskite/Spiro-OMeTAD/Au to obtain the trap density (n_{trap}) and charge-carrier mobility (μ) of the perovskite film. The *J*–*V* characteristics of the hole-only devices measured in the dark condition are shown in **Figure 6**. There are three different regions in the *J*–*V* curves: ohmic region, trap-filled limit (TFL) region and Child's region. The voltage between the ohmic and TFL regions is called the trap-filled limit voltage (V_{TFL}), which can be used to calculate the n_{trap} by using the following equation:[39,40]

$$V_{TFL} = \frac{e n_{trap} L^2}{2\varepsilon_0 \varepsilon}$$

Where ε_r is the dielectric constant of perovskite film, ε_0 is the vacuum permittivity, L is the thickness of perovskite layer, and e is the elementary charge. The trap density in the hole-only device prepared by the polymer containing anti-solvent is calculated to be 1.45×10^{16} cm^{-3}, which is lower than that of the hole-only device prepared by the CB anti-solvent, 1.91×10^{16} cm^{-3}, suggesting that polymer passivation can reduce the defects. In the high voltage Child's region, the current density-voltage curves can be fitted by using SCLC model:[40,41]

$$J = \frac{9}{8}\varepsilon_0 \varepsilon_r \mu \frac{V^2}{L^3}$$

where J and V are the measured current density and applied voltage, $\varepsilon_0\varepsilon_r$ is the permittivity of the component, μ is the charge carrier mobility and L is the thickness of perovskite layer. The hole-only devices prepared by the polymer containing anti-solvent have a hole mobility of 9.75×10^{-3} cm^2 V^{-1} s^{-1}, which is higher than that of the hole-only devices prepared by the CB anti-solvent, 7.67×10^{-3} cm^2 V^{-1} s^{-1}. The enhanced hole mobility and suppressed trap density in the hole-only device prepared by the polymer containing anti-solvent could be attributed to the passivation effect of the polymer in the perovskite film. The SCLC measurement results are also in good agreement with the TrPL results. With surface and GBs passivation, the charge carriers can be more efficiently transported from perovskite film to Spiro-OMeTAD, thus resulting in a higher charge carrier mobility and a better PSC performance.

Table 2. Summary of the parameters from fitting to the TrPL decay data.

Samples	A_1	τ_1 [ns]	A_2	τ_2 [ns]
Perovskite by CB anti-solvent	0.62	11.03	0.40	161.37
Perovskite by polymer containing anti-solvent	0.61	23.09	0.42	147.08
Perovskite by CB anti-solvent /Spiro-OMeTAD	0.24	4.23	0.71	31.88
Perovskite by polymer containing anti-solvent /Spiro-OMeTAD	0.53	1.86	0.54	21.99

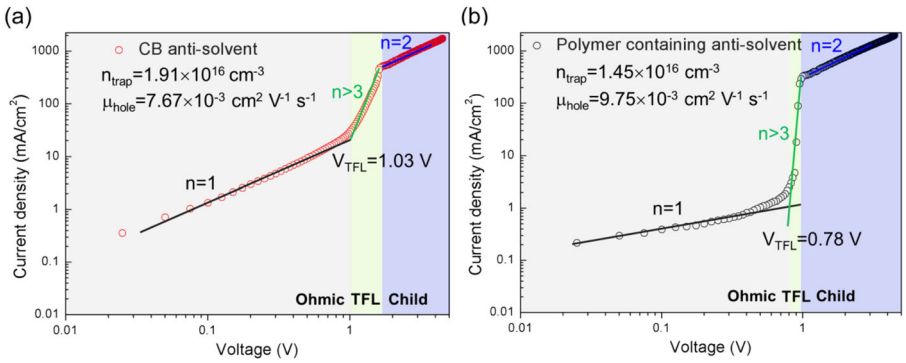

Figure 6. Current density-voltage characteristics of hole-only devices with structure of FTO/PEDOT:PSS/Perovskite/Spiro-OMETAD/Au prepared by the CB anti-solvent a) or the polymer containing anti-solvent b).

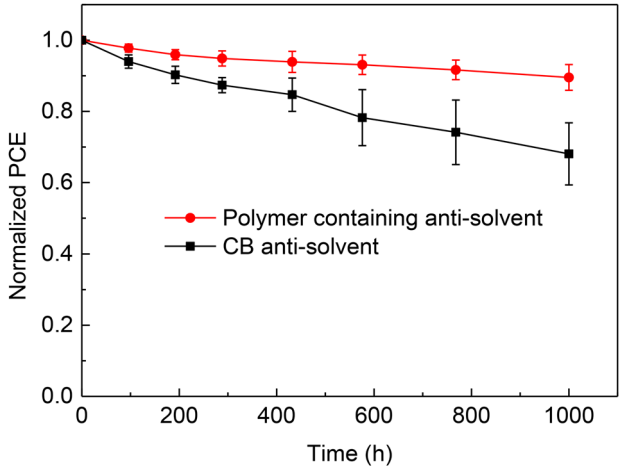

Figure 7. Normalized PCE of PSCs prepared by the CB anti-solvent and the polymer containing anti-solvent plotted as a function of storing time.

The stability of PSCs was investigated by storing the devices under ambient environment with 60% relative humidity in the dark at room temperature without encapsulation. The normalized PCE of PSCs prepared by the polymer containing anti-solvent and by the CB anti-solvent plotted as a function of storing time is shown in **Figure 7**. After storing for 1000 h, the PSCs prepared by the polymer containing anti-solvent retained 90% of the original PCE whereas the PCE of the PSCs prepared by the CB anti-solvent decreased to 68% of the original value. It has been widely reported that the defects could be a pathway for moisture to diffuse into perovskite film and accelerate the decomposition of perovskite crystals.[14,15] Therefore, the better stability of the PSCs prepared by the polymer containing anti-solvent can be attributed to the surface and GB passivation effect of PDTBDT-FBT in perovskite films.

3. Conclusions

In conclusion, we have improved the performance of PSCs by applying PDTBDT-FBT polymer dissolved in CB as an anti-solvent. After introducing the polymer containing anti-solvent in the preparation of perovskite films, the average PCE of PSCs was enhanced from 14.91 to 16.19% and the highest PCE of 18.03% was obtained. We thoroughly studied the mechanisms for performance improvement in PSCs and found that the introduced PDTBDT-FBT could passivate the surface and GBs of perovskite crystals, thus leading to the perovskite films with denser and more homogeneous morphology and indistinct GBs. The passivation effect of PDTBDT-FBT on perovskite crystals resulted in a faster charge transfer from perovskite to Spiro-OMeTAD. The PSCs prepared by the polymer containing anti-solvent also exhibited a better stability when storing in ambient environment with 60% humidity. Through this study, we demonstrated that dithieno-benzodithiophene-based π-conjugated polymers could be a promising material for passivation of perovskite. To further improve the performance of PSCs in future, more attentions should be paid to the passivation of defects.

4. Experimental Section

PSCs Fabrication: FTO glass substrates were sonicated sequentially with deionized water, acetone, and isopropanol for 10 min each followed by drying at 60 °C in an oven for several hours. The clean FTO glass substrates were exposed to ultraviolet light and ozone for 20 min before spin coating TiO_2 compact layer in argon filled glovebox. The TiO_2 compact layer precursor solution was prepared by diluting 1 mL titanium (IV) isopropoxide in 10 mL ethanol with 12 µL HCl (12 M). TiO_2 compact layer precursor solution was then spin coated on FTO glass substrates at 6000 rpm for 30 s followed by sintering at 450 °C for 20 min in air. After cooling down to room temperature, a mesoporous TiO_2 layer was deposited by spin coating a solution of TiO_2 paste (Dyesol, 30NR-D) in ethanol (150 mg mL^{-1}) at 4000 rpm with an acceleration of 2000 rpm s^{-1} for 20 s. The substrate with TiO_2 mesoporous layer was sintered at 450 °C for 20 min. The substrate was transferred into argon filled glovebox when it cooled down to 100 °C. The perovskite precursor solution was prepared by dissolving FAI (1 M), PbI_2 (1.1 M), MABr (0.2 M), and $PbBr_2$ (0.2 M) in anhydrous DMF:DMSO 4:1 (v:v).[19] A 42 µL CsI stock solution (1.5 M in DMSO) was added into 1 mL perovskite precursor solution to achieve the triple cation composition. The perovskite film was deposited by spin coating the perovskite precursor solution with CsI in a two steps program at 1000 and 6000 rpm for 10 and 20 s, respectively. During the second step, 110 µL of CB or polymer containing anti-solvent was poured on the spinning substrate 5 s prior to the end of the program. The polymer containing anti-solvent was prepared by dissolving PDTBDT-FBT (1-material) in CB and stirred at 70 °C for 1 h. After spin coating perovskite film, the substrates were annealed at 100 °C for 1 h in an argon filled glovebox. After annealing, a spiro-OMeTAD solution was spin coated at 3000 rpm for 30 s. The spiro-OMeTAD solution was prepared by dissolving 72 mg of spiro-OMeTAD in 1 mL of CB doped with 17.6 µL bis(trifluoromethylsulfonyl)imide lithium salt (Li-TFSI, 1.8 M in acetonitrile), 29.2 µL tris(2-(1H-pyrazol-1-yl)-4-tert-butylpyridine)-cobalt(III)

tris(bis(trifluoromethylsulfonyl)imide) (FK209, 100 mg mL^{-1} in acetonitrile) and 29.2 µL 4-tert-Butylpyridine (TBP). The device fabrication was completed by depositing 80 nm Au films on the spiro-OMeTAD film as top electrodes through a thermal evaporator at 3×10^{-4} Pa. The device active area was defined by a shadow mask to be 0.11 cm^2.

Hole-Only Device: The hole-only device with a structure of FTO/PEDOT:PSS/perovskite/Spiro-OMeTAD/Au was fabricated by spin coating PEDOT:PSS (Al 4083) solution filtered through 0.45 µm PVDF filter on UV-ozone treated FTO substrate at 3000 rpm for 50 s followed by annealing at 130 °C for 15 min. The perovskite films were prepared by CB or polymer containing anti-solvent (1 mg mL^{-1} PDTBDT-FBT in CB) followed by annealing at 100 for 1 h. Then Spiro-OMeTAD was spin coated on top of perovskite film. The hole-only device was completed by depositing Au top electrodes by using a thermal evaporator. The preparation of perovskite and Spiro-OMeTAD layers followed the same procedure described in PSCs fabrication.

Characterization: The current density-voltage (*J*–*V*) characteristics of PSCs were measured by a Keithley 2400 parameter analyzer under 1 sun solar spectrum illumination (AM 1.5 G) from a solar simulator with intensity of 100 mW cm^{-2} calibrated via a silicon reference cell. EQE measurements were conducted on devices under short-circuit conditions through a lock-in amplifier under illumination with a monochromatic light from a xenon arc lamp. The devices were measured in ambient environment without encapsulation. UV-Vis absorption spectra were performed on a PERSEE TU-1901 spectrophotometer. XRD patterns were collected using a Rigaku SmartLab 9 kW system with Cu-Kα radiation. X-ray photoelectron spectroscopy (XPS) was obtained on an XlESCALAB 250Xi electron spectrometer from VG Scientific with a monochromatic Al K radiation. SEM images were characterized by Zeiss Merlin scanning electron microscope. Time-resolved PL spectra were recorded by Edinburgh FS-5 spectrometer equipped with the excitation source of 450 nm pulsed laser.

Supporting Information

Supporting Information is available from the Wiley Online Library or from the author.

Acknowledgements

This work was supported by the start-up funds from Thousand Young Talents Program and Shenzhen Municipal Science and Technology Innovation Committee. X. W. Sun acknowledges the support from the National Key Research and Development Program of China administrated by the Ministry of Science and Technology of China (No. 2016YFB0401702), National Natural Science Foundation of China (No. 61674074), Shenzhen Peacock Team Project (No. KQTD2016030111203005), and Shenzhen Innovation Project (No. JCYJ20160301113356947). G. Li thanks for the National Science Foundation of China (51773091, 61604069, and 61761136013).

Conflict of Interest

The authors declare no conflict of interest.

Keywords

anti-solvent, passivation, perovskite solar cell

Received: January 22, 2019
Revised: February 15, 2019
Published online:

[1] P. Docampo, J. M. Ball, M. Darwich, G. E. Eperon, H. J. Snaith, *Nat. Commun.* **2013**, *4*, 6.
[2] Y. Li, L. Meng, Y. Yang, G. Xu, Z. Hong, Q. Chen, J. You, G. Li, Y. Yang, Y. Li, *Nat. Commun.* **2016**, *7*, 10.
[3] X. Li, X. Tang, T. Ye, D. Wu, H. Wang, X. Wang, *ACS Appl. Mater. Interfaces* **2017**, *9*, 18730.
[4] A. Kojima, K. Teshima, Y. Shirai, T. Miyasaka, *J. Am. Chem. Soc.* **2009**, *131*, 6050.
[5] NREL chart, https://www.nrel.gov/pv/assets/pdfs/pv-efficiency-chart. 2019 0103.pdf.
[6] X. Li, D. Bi, C. Yi, J. D. Decoppet, J. Luo, S. M. Zakeeruddin, A. Hagfeldt, M. Gratzel, *Science* **2016**, *353*, 58.
[7] Y. Wu, X. Yang, W. Chen, Y. Yue, M. Cai, F. Xie, E. Bi, A. Islam, L. Han, *Nat. Energy* **2016**, *1*, 16148.
[8] W. S. Yang, J. H. Noh, N. J. Jeon, Y. C. Kim, S. Ryu, J. Seo, S. I. Seok, *Science* **2015**, *348*, 1234.
[9] Y. Jiang, E. J. Juarez-Perez, Q. Ge, S. Wang, M. Leyden, L. Ono, S. Raga, J. Hu, Y. Qi, *Mater. Horizons* **2016**, *3*, 548.
[10] D. W. deQuilettes, S. M. Vorpahl, S. D. Stranks, H. Nagaoka, G. E. Eperon, M. E. Ziffer, H. J. Snaith, D. S. Ginger, *Science* **2015**, *348*, 683.
[11] K. Zhu, T. Miyasaka, J. Y. Kim, I. Mora-Sero, *J. Phys. Chem. Lett.* **2015**, *6*, 2315.
[12] M. J. Simpson, B. Doughty, B. Yang, K. Xiao, Y. Ma, *J. Phys. Chem. Lett.* **2016**, *7*, 1725.
[13] O. G. Reid, M. J. Yang, N. Kopidakis, K. Zhu, G. Rumbles, *ACS Energy Lett.* **2016**, *1*, 561.
[14] Q. Wang, B. Chen, Y. Liu, Y. Deng, Y. Bai, Q. Dong, J. Huang, *Energy Environ. Sci.* **2017**, *10*, 516.
[15] Y. Shao, Y. Fang, T. Li, Q. Wang, Q. Dong, Y. Deng, Y. Yuan, H. Wei, M. Wang, A. Gruverman, J. Shielda, J. Huang, *Energy Environ. Sci.* **2016**, *9*, 1752.
[16] N. Faraji, C. J. Qin, T. Matsushimia, C. Adachi, J. Seidel, *J. Phys. Chem. C* **2018**, *122*, 4817.
[17] L. Liu, S. Huang, Y. Lu, P. Liu, Y. Zhao, C. Shi, S. Zhang, J. Wu, H. Zhong, M. Sui, H. Zhou, H. Jin, Y. Li, Q. Chen, *Adv. Mater.* **2018**, *30*, 8.
[18] T. Niu, J. Lu, R. Munir, J. Li, D. Barrit, X. Zhang, H. Hu, Z. Yang, A. Amassian, K. Zhao, S. Liu, *Adv. Mater.* **2018**, *30*, 11.
[19] M. Saliba, T. Matsui, J. Y. Seo, K. Domanski, J. P. Correa-Baena, M. K. Nazeeruddin, S. M. Zakeeruddin, W. Tress, A. Abate, A. Hagfeldt, M. Gratzel, *Energy Environ. Sci.* **2016**, *9*, 1989.
[20] T. Bu, X. Liu, Y. Zhou, J. Yi, X. Huang, L. Luo, J. Xiao, Z. Ku, Y. Peng, F. Huang, Y. Cheng, J. Zhong, *Energy Environ. Sci.* **2017**, *10*, 2509.
[21] K. T. Cho, S. Paek, G. Grancini, C. Roldan-Carmona, P. Gao, Y. H. Lee, M. K. Nazeeruddin, *Energy Environ. Sci.* **2017**, *10*, 621.
[22] N. J. Jeon, J. H. Noh, Y. C. Kim, W. S. Yang, S. Ryu, S. I. Seok, *Nat. Mater.* **2014**, *13*, 897.
[23] D. Bi, C. Yi, J. Luo, J. D. Decoppet, F. Zhang, S. M. Zakeeruddin, X. Li, A. Hagfeldt, M. Gratzel, *Nat. Energy* **2016**, *1*, 5.
[24] J. Luo, J. Xia, H. Yang, L. Chen, Z. Wan, F. Han, H. A. Malik, X. Zhu, C. Jia, *Energy Environ. Sci.* **2018**, *11*, 12.
[25] P. Qin, G. Yang, Z. Ren, S. H. Cheung, S. K. So, L. Chen, J. Hao, J. Hou, G. Li, *Adv. Mater.* **2018**, *30*, 12.
[26] W. Zhao, S. Li, H. Yao, S. Zhang, Y. Zhang, B. Yang, J. Hou, *J. Am. Chem. Soc.* **2017**, *139*, 7148.
[27] W. Zhong, J. Xiao, S. Sun, X. Jiang, L. Lan, L. Ying, W. Yang, H. Yip, F. Huang, Y. Cao, *J. Mater. Chem. C* **2016**, *4*, 4719.
[28] P. Guo, G. Luo, Q. Su, J. Li, P. Zhang, J. Tong, C. Yang, Y. Xia, H. Wu, *ACS Appl. Mater. Interfaces* **2017**, *9*, 10937.
[29] C. Zhang, M. Li, Z. Wang, Y. Jiang, H. Liu, Y. Yang, X. Gao, H. Ma, *J. Mater. Chem. A* **2017**, *5*, 2572.
[30] A. Privitera, M. Righetto, M. De Bastiani, F. Carraro, M. Rancan, L. Armelao, G. Granozzi, R. Bozio, L. Franco, *J. Phys. Chem. Lett.* **2017**, *8*, 5981.

[31] Y. Wu, P. Wang, X. Zhu, Q. Zhang, Z. Wang, Y. Liu, G. Zou, Y. Dai, M. H. Whangbo, B. Huang, *Adv. Mater.* **2018**, *30*, 6.
[32] N. Krishnamurthy, V. Soots, *Can. J. Phys.* **1970**, *48*, 1104.
[33] M. Liu, L. Zhao, Y. Liu, Z. Lan, L. Chang, Y. Li, H. Yu, *J. Mater. Sci. Technol.* **2014**, *30*, 1213.
[34] G. R. Perumallapelli, S. R. Vasa, J. Jang, *Org. Electron.* **2016**, *31*, 142.
[35] A. Nawaz, A. K. Erdinc, B. Gultekin, M. Tayyib, C. Zafer, K. Y. Wang, M. N. Akram, K. K. Wong, S. Hussain, L. Schmidt-Mende, A. Fakharuddin, *J. Mater. Sci-mater. El* **2017**, *28*, 15630.
[36] S. R. Pathipati, M. N. Shah, *Sol. Energy* **2018**, *162*, 8.
[37] G. Grancini, A. R. S. Kandada, J. M. Frost, A. J. Barker, M. De Bastiani, M. Gandini, S. Marras, G. Lanzani, A. Walsh, A. Petrozza, *Nat. Photonics* **2015**, *9*, 695.
[38] Z. Zhu, Y. Bai, H. K. H. Lee, C. Mu, T. Zhang, L. Zhang, J. Wang, H. Yan, S. K. So, S. Yang, *Adv. Funct. Mater.* **2014**, *24*, 7357.
[39] Z. Liu, J. Hu, H. Jiao, L. Li, G. Zheng, Y. Chen, Y. Huang, Q. Zhang, C. Shen, Q. Chen, H. Zhou, *Adv. Mater.* **2017**, *29*, 8.
[40] Y. Guo, J. Ma, H. Lei, F. Yao, B. Li, L. Xiong, G. Fang, *J. Mater. Chem. A* **2018**, *6*, 5919.
[41] H. J. Park, M. G. Kang, S. H. Ahn, L. Guo, *Adv. Mater.* **2010**, *22*, E247.